Monthly Notices
of the
ROYAL ASTRONOMICAL SOCIETY

Mon. Not. R. Astron. Soc. **401,** 1796–1803 (2010) doi:10.1111/j.1365-2966.2009.15742.x

The birth and growth of neutralino haloes

R. E. Angulo★ and S. D. M. White

Max-Planck-Intitute fur Astrophysik, D-85741 Garching, Germany

Accepted 2009 September 16. Received 2009 September 16; in original form 2009 June 9

ABSTRACT

We use the extended Press–Schechter (EPS) formalism to study halo assembly histories in a standard Λ cold dark matter cosmology. A large ensemble of Monte Carlo random walks provides the *entire* halo membership histories of a representative set of dark matter particles, which we assume to be neutralinos. The first-generation haloes of most particles do not have a mass similar to the free-streaming cut-off $M_{\rm fs}$ of the neutralino power spectrum, nor do they form at high redshift. Median values are $M_1 = 10^5$–$10^7 M_{\rm fs}$ and $z_1 = 13$ to 8 depending on the form of the collapse barrier assumed in the EPS model. For almost one third of all particles, the first-generation halo has $M_1 > 10^9 M_{\rm fs}$. At redshifts beyond 20, most neutralinos are not yet part of any halo but are still diffuse. These numbers apply with little modification to the neutralinos which are today part of haloes similar to that of the Milky Way. Up to 10 per cent of the particles in such haloes were never part of a smaller object; the typical particle has undergone approximately five 'accretion events' where the halo it was part of falls into a more massive object. Available N-body simulations agree well with the EPS predictions for an 'ellipsoidal' collapse barrier, so these may provide a reliable extension of simulation results to smaller scales. The late formation times and large masses of the first-generation haloes of most neutralinos suggest that they will be disrupted with high efficiency during halo assembly.

Key words: cosmology: theory – large-scale structure of Universe.

1 INTRODUCTION

The existence of 'cold dark matter (CDM)' is one of the pillars of our current understanding of the origin and evolution of structure in our Universe. Many independent astrophysical observations have not only provided evidence of its existence but also indications of its properties; the CDM particle should be non-baryonic, collisionless, neutral and with small initial velocities. In spite of the arguments supporting such a particle, no member of the standard model of particle physics can fit the requirements. Fortunately, this problem is 'solved' in supersymmetric extensions where many candidate particles for CDM emerge. In particular, the lightest neutralino, which should have a mass of about 100 GeV, is the currently favoured choice, as it is both weakly interacting and stable (see Bertone, Hooper & Silk 2005, for a review of current candidates).

Some properties of the neutralino, such as its mass, have a direct impact on the formation and evolution of structure in the Universe. The finite temperature at which these particles decouple from the radiation field before recombination imprints features in the primordial power spectrum of fluctuations at very small scales. In particular, the free streaming of neutralinos suppresses perturbations with comoving scale in the range 0.01–100 pc depending on particle properties, implying that objects collapse gravitationally only above a corresponding free-streaming mass $M_{\rm fs}$, with $10^{-12} < M_{\rm fs} < 10^{-2}\,{\rm M}_\odot$. Naturally, this significantly affects the properties of the first objects in the Universe, which must have masses comparable to, or larger than, $M_{\rm fs}$. The free streaming of neutralinos may also modify the way in which much larger haloes grow. For example, the amount of mass that a halo accretes in diffuse form depends on how much mass in the Universe is in collapsed objects. The objective of this paper is to study these and other aspects of structure formation in a Λ-neutralino cosmology.

The most accurate way to study the highly non-linear dynamics involved in the formation and evolution of haloes is via N-body simulations. However, resolving galactic haloes and objects with $M \sim M_{\rm fs}$ simultaneously poses an extremely hard problem that is currently impossible to solve. For example, for $M_{\rm fs} \sim 10^{-8}\,{\rm M}_\odot$ a direct N-body simulation of the Milky Way's halo would require at least 10^{23} particles, almost 14 orders of magnitude larger than the most sophisticated simulations performed so far. Extrapolating Moore's law, such calculation may become possible after the year 2050.

So far, several different approaches have been used in the literature to study the implications of neutralinos for early structure formation. One consists in simulating scale-free cosmologies. There, the initial power spectrum is assumed to be a power law, with index similar to that of CDM on very small scales. Although the range of scales is no larger than in a standard CDM simulation, it superficially appears possible to study the formation of very small haloes,

★E-mail: reangulo@mpa-garching.mpg.de

with masses similar to the free-streaming cut-off mass (e.g. Widrow et al. 2009). The weakness of such simulations is that the results are not properly coupled to the evolution of longer wavelength perturbations; as we will see below, these are actually very important in a realistic CDM cosmology. Another tactic is to resimulate extremely low-density regions at very high resolution in such way that the Lagrangian region of the simulation is confined to a small zone and the mass of each simulation particle can be very small (e.g. Diemand, Moore & Stadel 2005). This approach is intrinsically limited to unrepresentative regions of the very high-redshift Universe. Yet another tactic is to carry out a set of nested zoomed simulations (Gao et al. 2005b) although this technique has yet to be extended all the way to the free-streaming mass.

In this paper, we adopt a less accurate but self-consistent strategy based on excursion set theory (Press & Schechter 1974; Bond et al. 1991; Bower 1991; Lacey & Cole 1993). This formalism has been extremely successful in reproducing many aspects of dark matter halo formation, as well as in fitting halo mass distributions and clustering. It provides a realistic model for halo growth over its entire history. Although the theory has not been tested on very small scales, it is currently the only way to compute the *full* mass assembly history of present-day haloes, i.e. starting from the free-streaming mass, the very bottom of the CDM hierarchy and following growth up to cluster scales the largest collapsed objects in the Universe.

This paper is organized as follows. First, we illustrate how the free streaming of neutralinos modifies the primordial density field. In Section 3, we provide the theoretical background and the tools necessary for our analysis. We discuss our first results in Section 4, where we investigate the typical redshift at which dark matter particles become part of a halo for the first time, as well as the mass of those haloes. We then move to Section 5 where we look at the assembly history of a Milky Way sized halo. We present some final remarks in Section 6.

Note that throughout this paper we will use the following cosmological model: matter density parameter, $\Omega_{\rm M} = 0.25$; vacuum energy density parameter, $\Omega_\Lambda = 0.75$; normalization of density fluctuations, expressed in terms of the extrapolated linear amplitude of density fluctuations in spheres of radius $8\,h^{-1}$ Mpc at the present day, $\sigma_8 = 0.9$; primordial spectral index $n_{\rm s} = 1$ and the Hubble constant, $H_0 = 73\,{\rm km\,s^{-1}\,Mpc^{-1}}$. We will also, in general, adopt a standard neutralino with mass 100 GeV, corresponding to $M_{\rm fs} \sim 10^{-8}\,{\rm M}_\odot$.

2 NEUTRALINO CDM POWER SPECTRUM

In the classical ΛCDM model, the density fluctuations increase monotonically with wavenumber. However, this behaviour is modified by neutralino streaming. The properties of the neutralino set the temperature at which the population becomes non-relativistic. This moment sets the primordial velocity dispersion of neutralinos and characterizes the scale below which perturbations are suppressed. Roughly speaking, any perturbation smaller than the mean free path of neutralinos over a Hubble time will be dissipated, producing a cut-off in the primordial power spectrum.

We can see this effect quantitatively in Fig. 1. This plot shows the neutralino–CDM power spectrum predicted by linear perturbation theory. The corresponding variance of the linear density field, extrapolated to $z = 0$, in spheres of different radius (and hence enclosed mass) is shown in Fig. 2. We have computed fluctuations on large scales using the Boltzmann code CAMB (Lewis, Challinor & Lasenby 2000) whilst on very small scales the power spectrum is that predicted by the approach of Green, Hofmann & Schwarz (2004) which includes effects from the free streaming of neutralinos. Note that calculating the effects of free streaming requires considerable care to obtain accurate results (e.g. Green et al. 2004; Loeb & Zaldarriaga 2005; Bertschinger 2006; Bringmann 2009). As we will show below, however, our main results are extremely insensitive to $M_{\rm fs}$, so the details do not matter much for our purposes.

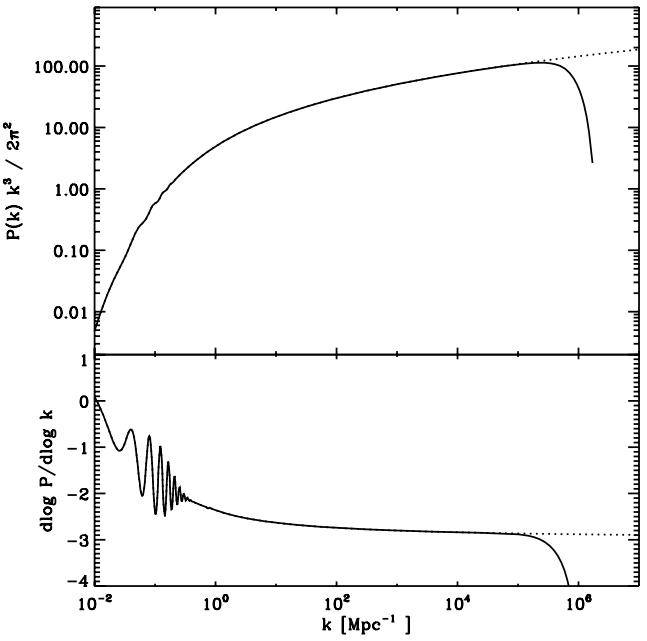

Figure 1. Top panel: the dimensionless power spectrum of the dark matter density field at $z = 0$ predicted by linear perturbation theory. Bottom panel: the logarithmic derivative of the power spectrum, i.e. the local power-law index of the power spectrum. The solid line shows the power spectrum assuming that the dark matter particles are neutralinos of mass 100 GeV whilst the dashed lines effectively assume an infinite mass for the dark matter particle.

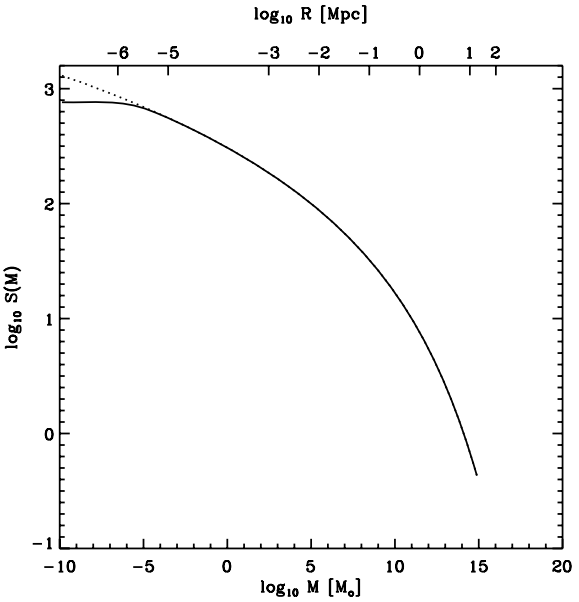

Figure 2. The logarithm of the $z = 0$ mass variance $S(M)$ smoothed with a real space top-hat filter as a function of the smoothing radius (mass) normalized to $\sigma_8 = 0.9$. The solid lines take into account the cut-off in the power spectrum for 100 GeV neutralinos.

In both figures, solid lines assume a neutralino of mass 100 GeV and a temperature at kinetic decoupling of 33 MeV. As previously discussed, free streaming suppresses the power on very small scales ($R_{\rm fs} \sim 0.5\,h^{-1}$ pc) generating an exponential cut-off. The counterpart of the lack of power on small scales is a flattening of the variance for very small smoothing radii. Thus, there is a finite maximum variance of the field which, for our cosmological model, is equal to ∼760. For comparison, we have also included the prediction for a very massive CDM particle which is displayed as dotted lines. In this case, there is no suppression of fluctuations and the variance diverges logarithmically as the slope of the power spectrum approaches −3.

The features introduced by the neutralino have immediate implications for structure formation. For instance, the smallest possible dark matter objects in the Universe have a mass $\sim 10^{-8}\,{\rm M}_\odot$ (1 per cent of the mass of the Earth) and the most abundant haloes are predicted by excursion set theory to have masses typically of the order of $10^{-6}\,{\rm M}_\odot$.

The existence of a minimum halo mass in the Universe does not, however, imply that most of the dark matter was once part of such an object. Indeed, as we will show in subsequent sections, only a small fraction of neutralinos were ever part of such haloes. Before we investigate this and related issues in more detail, the following section gives a brief overview of the techniques that will make our analysis possible.

3 METHODOLOGY

We start this section by reviewing excursion set theory and the various collapse models that are used as part of it. We also discuss our practical implementation of the formalism. Finally, we provide a description of the *N*-body simulation with which we will test some of our results.

3.1 The excursion set approach to the formation and evolution of haloes

Dark matter haloes are highly non-linear objects. In spite of their complexity, many of their statistical properties can be described surprisingly well by the simple analytical arguments of excursion set theory. In the following, we will give a brief summary of the main ideas behind the model, a comprehensive review is given by Zentner (2007).

The classic implementation of excursion set theory (Bond et al. 1991; Bower 1991; Lacey & Cole 1993) starts by considering a random particle and then smoothing the density contrast field around it on progressively smaller scales until its smoothed overdensity crosses a threshold for collapse. The particle then is assumed to belong to a halo of Lagrangian mass equal to that enclosed in the smoothing window at threshold.

In practice, the smoothed density contrast is generated by convolving the density contrast field with a smoothing window, W,

$$\delta_R(\boldsymbol{x}) = \int \delta(\boldsymbol{x}')W(\boldsymbol{x}-\boldsymbol{x}';R){\rm d}^3x'. \quad (1)$$

On the same scale, the total variance of the field, $S(R)$, is

$$S(R) \equiv \left\langle \delta_R^2 \right\rangle = \frac{1}{2\pi^2}\int {\rm d}k k^2 P(k)\widetilde{W}^2(k;R), \quad (2)$$

where $P(k)$ is the dark matter power spectrum discussed in the previous section. An extremely interesting filter is a top-hat in Fourier space, where $\widetilde{W}(k;R) = 1$ for all points with $k \leq R^{-1}$ and $\widetilde{W}(k;R) = 0$ otherwise. In this case, the smoothed density contrast executes a Markov random walk in the $S-\delta$ plane as R decreases, since increasing the window adds wave modes that are independent of those previously included.

Once we have computed the trajectory $\delta(S)$ for each particle, the next step is to associate the particle to a collapsed object. The simplest criterion for collapse is that a dark matter particle is considered part of a halo with mass M, such that the density contrast smoothed on the scale $R(M)$ first exceeds some critical value. The relation between R and M is given by the volume enclosed in the smoothing window.

The critical overdensity for collapse at a given redshift may be taken as constant or as function of the variance; these are known as constant and moving barriers, respectively. The first is motivated by the spherical collapse model, which predicts that at the moment of virialization the linearly extrapolated density contrast is $\delta_{\rm sc} \sim 1.686$. On the other hand, the moving barriers approximately account for the fact that, in order to collapse, a small perturbation must have a higher density contrast compared with a larger perturbation because it is typically more asymmetrical. These barriers are motivated by ellipsoidal collapse models and they are usually taken to have the following form:

$$\delta_{\rm c}(S,z) = \sqrt{q}\delta_{\rm sc}\left[1+\beta\left(\frac{S}{q\delta_{\rm sc}^2}\right)^\gamma\right], \quad (3)$$

where, by using the expectation value for the shape of dark matter haloes as a function of scale, a single condition (depending only on the variance of the field) can be applied to all trajectories at a given redshift.

By analysing the criteria for collapse for an ensemble of walks as a function of redshift, the excursion set formalism predicts the probability distribution of halo assembly histories for an ensemble of DM particles.

Despite the simplicity of the argument, the excursion set approach has been extremely successful in reproducing many properties of DM haloes as determined from *N*-body simulations. In particular, the clustering and number density of haloes are well reproduced, as is the mass function of their progenitors. Nevertheless, the approach fails to reproduce all results from simulations, e.g. the dependence of clustering on halo properties other than mass (Gao, Springel & White 2005a; Wechsler et al. 2006; Gao & White 2007; Wetzel et al. 2007; Angulo, Baugh & Lacey 2008a). This particular disagreement arises because the Markov nature of the overdensity trajectories implies that there can be no correlation between the assembly history of a halo and its large-scale environment (White 1996). Such a dependence is, however, found in simulations.

3.2 Monte Carlo simulations

We have implemented the ideas described in the previous section as follows. First, we compute the smoothing radii for which we will generate each random walk. These have a variable spacing in mass given by the condition $M_i = 0.9M_{i-1}$. This choice ensures that we can easily resolve all the events where the halo associated with a random walk increases its mass by a factor of 2, allowing us to resolve all infall events and major mergers. The probability that at a given radius R_i the smoothed field has a value between δ and $\delta + {\rm d}\delta$ is then given by $\exp[(\delta-\delta_{\rm i-1})^2/S(R_i)]{\rm d}\delta$. Note that the choice of $R_{i=0}$ does not affect our results, as long as it is smaller than the cut-off scale. This is due to the fact that the variance does not change below the cut-off scale, i.e. $S(r_1) = S(r_{\rm fs})$ for $r_1 < r_{\rm fs}$.

Any perturbation above the critical density, δ_c, at r_1 will necessarily also be above δ_c at R_{fs}. In practice, we chose $R_{i=0} = 0.1 \times R_{fs}$.

This approach, combined with the maximum finite variance of the field (cf. Section 2), implies that only ∼2000 random numbers are necessary to follow the complete assembly history of the haloes associated with a particular dark matter particle over the 25 orders of magnitude which separate the smallest halo it could possibly reside in from a M_* halo today.

At each step of the random walks, we check whether a collapse criterion is fulfilled or not. We considered both the constant spherical collapse barrier and a square root barrier for which $(q, \beta, \gamma) = (0.5, 0.55, 0.5)$ in equation (3). Note that the latter set of parameters ensures that barriers at different redshift will never intersect each other, as can happen, for instance, for the ellipsoidal barrier that best reproduces mass functions in N-body simulations (Sheth, Mo & Tormen 2001; Mahmood & Rajesh 2005; Moreno, Giocoli & Sheth 2008).

We have used two different starting points for the density and variance. First, we set $(S, \delta)_{i=0} = (0, 0)$ so the trajectories represent a random set of CDM particles. These walks allow us to investigate general properties of dark matter haloes which will be presented in Section 5. The second starting point is $(S, \delta)_{i=0} = (4.96, 1.686)$ and $(S, \delta)_{i=0} = (4.96, 2.36)$ for the spherical collapse and square root barrier, respectively, which generates trajectories that represent CDM particles that end up in a Milky Way sized halo today. In this way, we can look into the properties of the mass assembly of such haloes. We will analyse these in Section 6.

We repeat our algorithm 10^5 times to generate a large ensemble of random walks. This allow us to represent the probability distribution of halo mass assembly histories for neutralinos in a ΛCDM Universe.

3.3 The hMS simulation

The smallest haloes that can be resolved in current N-body simulations are many orders of magnitude more massive than the smallest haloes expected in a neutralino-CDM Universe. Nevertheless, by imposing on our random walks an artificial minimum halo mass that matches the resolution of an N-body simulation, we can quantitatively assess the performance of the excursion set approach.

The N-body simulation we have chosen to compare our results with is the hMS presented in Angulo et al. (2008b). This simulation used 900^3 particles, each of mass $1.3 \times 10^8\,M_\odot$, to follow the gravitational dynamics of the dark matter distribution within a periodic box of side 137 Mpc. It is a lower resolution version of the Millennium-II Simulation of Boylan-Kolchin et al. (2009) and has the same set of cosmological parameters as used in the Millennium Simulation of Springel (2005).

Every ∼100 Gyr we have identified haloes using a friends-of-friends (FoF) algorithm (Davis et al. 1985) as well as substructures within them using the SUBFIND procedure described in Springel et al. (2001). We have found the progenitors and descendant of every halo by following its 10 per cent most bound particles between snapshots, as described in Angulo et al. (2008b). The combination of high resolution in mass and a considerable volume allows us to sample the evolution of dark matter particles over a wide range of halo mass.

4 THE FIRST OBJECTS IN THE UNIVERSE

In this section, we present statistics for the first haloes occupied by typical DM particles based on our ensemble of random walks.

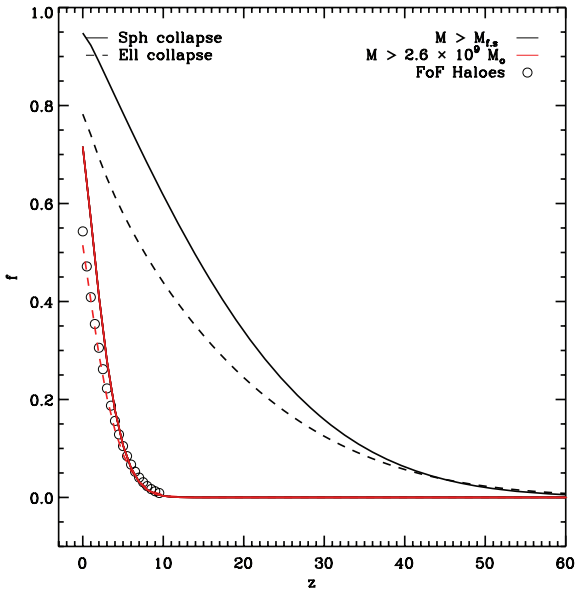

Figure 3. The fraction of mass in collapsed objects of any mass (black curves) and above a mass of $2.6 \times 10^9\,M_\odot$ (red curves) as a function of redshift. The results displayed as solid lines are computed using a constant barrier while the dashed lines are computed using a square root barrier. Measurements from an N-body simulation are also displayed as black circles. Note that the black lines assume no cut other than that imposed by the nature of the neutralino.

In particular, we will show the total mass fraction in haloes of *any* mass, and the distribution of mass and redshift at which typical neutralinos become part of a halo for the first time.

4.1 The mass in collapsed objects

Fig. 3 shows as a function of redshift, the fraction of random walks that have ever crossed the threshold for collapse, as well as the fraction that cross for a value of the smoothing mass greater than $2.6 \times 10^9\,M_\odot$. These curves correspond to the fraction of all cosmic matter in haloes of *any* mass, and in haloes above $2.6 \times 10^9\,M_\odot$.

A common misconception is that in CDM models every DM particle belongs to a halo of some mass. Fig. 3 clearly contradicts this. The fluctuation cut-off induced by neutralino streaming implies that some trajectories never cross the critical threshold for collapse. As we follow trajectories down to smaller smoothing masses, the fraction that have crossed the threshold asymptotes to values smaller than unity. The asymptotic value depends on the shape of the barrier. The fraction of all matter predicted to be in diffuse form at $z = 0$, i.e. to be part of no clump, is 5 and 22 per cent for constant and square root barriers, respectively.

This effect is stronger at high redshift where a much lower fraction of DM is part of haloes. Less than half of the mass is in any halo beyond redshifts 7.8 and 13.8 for the ellipsoidal and spherical models, respectively. By $z \sim 34$, the fraction of diffuse mass has reached 90 per cent in both models. Finally, beyond $z \sim 60$ less than 1 per cent of the mass is in gravitationally bound structures.

Black circles in Fig. 3 show the fraction of DM particles associated to FoF haloes (identified with at least 20 particles) in the hMS simulation. This can be compared directly with the red lines which indicate the fraction of random walks in haloes above the corresponding mass limit $M > 2.6 \times 10^9\,M_\odot$. For the square root barrier, 49.4 per cent of the random walks are associated with such

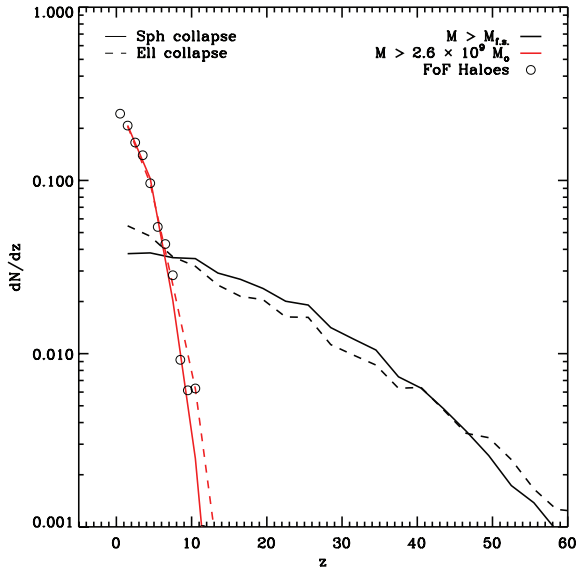

Figure 4. The distribution of redshifts at which DM particles are accreted on to a halo of any mass (black curves) or on to haloes more massive than $2.6 \times 10^9\,\mathrm{M}_\odot$ (red curves). *N*-body simulation results are shown as open circles.

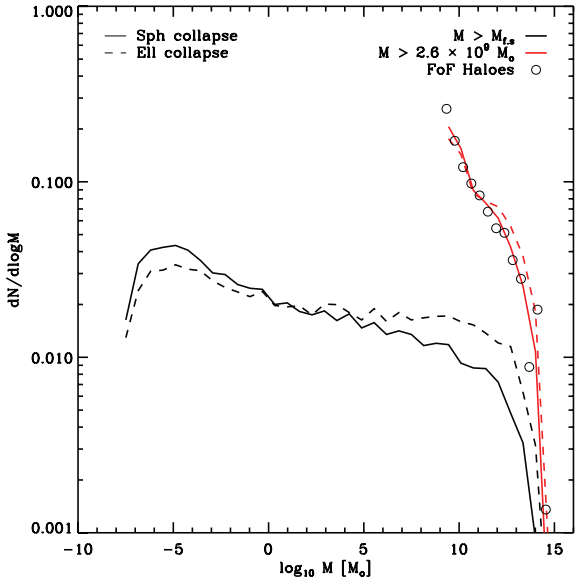

Figure 5. The mass distribution at first threshold crossing. The solid and dashed lines indicate the results for constant and moving collapse barriers, respectively. Note that the statistics only include the trajectories that do eventually fulfil the criterion for collapse; hence, the area below each curve is 1.

haloes at $z = 0$, this is very close to the fraction of the particles found in FoF haloes (54.3 per cent). A larger difference exists with the spherical model which overestimates the mass fraction in haloes at redshift zero by roughly 30 per cent. In general, however, the agreement with the two models is quite good.

4.2 The mass and redshift distribution of first objects

In Fig. 4, we present the distribution of the redshift at which the threshold is first crossed for the random walks that end up in some halo at $z = 0$. This corresponds to the differential probability that a halo particle first becomes part of a collapsed object at redshift z.

If we assume the ellipsoidal model for collapse (the dashed lines), the median value of the distribution is $z = 10.65$, and 90 per cent of the crossings occur at redshifts lower than 35.2. For the spherical collapse (solid lines) these redshifts are modified to $z = 12.8$ and 33.8, respectively. Thus, less than half of the neutralinos that are part of DM haloes today were part of any halo at $z = 13$. Less than 10 per cent of the mass in today's haloes was already in a halo of any mass by redshift 36.

Fig. 5 shows the distribution of the halo masses at which these first barrier crossings occur. This plot thus displays the probability per logarithmic mass interval that a neutralino that is part of a halo today was first accreted in diffuse form on to a halo of mass M. This is equivalent to the mass distribution of the first haloes of randomly chosen DM particles from present-day haloes.

Because of the shallow slope of the variance at small radii (Fig. 2), the distribution of masses shown in Fig. 5 is extremely flat; it varies by a factor of $\sim$3 across $\sim$20 orders of magnitude in mass. As a result, the first halo mass for DM particles is very diverse. Median values of the distribution are $\sim 10^{-2}$ and $1.4\,\mathrm{M}_\odot$ for the constant and moving barrier, respectively. Most neutralinos were never part of a halo of mass $M < 10^5\,M_{\rm fs}$. In fact, only 10 per cent were ever part of an object smaller than Earth mass, the same mass fraction for which the first halo was more massive than $\sim 10^7\,\mathrm{M}_\odot$.

Further results from our random walks are that the median redshift of collapse of 'first' objects of mass smaller than $10^{-4}\,\mathrm{M}_\odot$ is 24.1, only slightly larger than that of objects in the range 10^{-2}–$10^2\,\mathrm{M}_\odot$ which is $z = 15.8$. This suggest that the concentration of the smallest objects in the CDM hierarchy should not be significantly greater than that of objects thousands of times more massive. Thus, we may expect that most objects with mass $M \sim M_{\rm fs}$ are efficiently disrupted by tidal forces as they merge into more massive haloes in the same way as other more massive haloes formed at similar redshift (e.g. Springel et al. 2008). Addressing this question quantitatively will require a dedicated simulation programme.

Naturally, there is a correlation between mass and redshift at first threshold crossing. The higher the redshift of collapse, the smaller the typical halo mass. For example, the median first halo mass for trajectories which first cross threshold before $z = 10$ is $10^{-3}\,\mathrm{M}_\odot$ while for those first crossing before $z = 20$ it is $10^{-4}\,\mathrm{M}_\odot$. This reflects the increase in variance to smaller scales seen in Fig. 2.

In Figs 4 and 5, measurements from the hMS simulation are compared with excursion set predictions, where we have imposed an artificial mass cut to match the resolution of the *N*-body simulation (red lines). The simulated redshift and mass distributions for these 'first' objects agree well with those predicted by the excursion set formalism. This motivates our extrapolation of the predictions down to scales where the theory has not yet been tested. Nevertheless, it is important to keep in mind that this is an aggressive extrapolation.

In the final part of this section, we investigate the sensitivity of our results to changes in the free-streaming mass ($M_{\rm fs}$) and in the spectral index of the primordial power spectrum ($n_{\rm s}$). At given smoothing scale, the fluctuation amplitude increases with $n_{\rm s}$, producing a larger fraction of trajectories which have crossed the threshold for collapse. Hence, first threshold crossing is typically at higher redshift and at lower mass. On the other hand, decreasing $M_{\rm fs}$ allows smaller objects to form and thus typically decreases the halo mass and increases the redshift at first barrier crossing.

In order to quantify these effects, we repeated our calculations for the square root barrier using values of $n_{\rm s}$ ranging from 1.05 to 0.95, and of $M_{\rm fs}$ ranging from 10^{-14} to $10^{-4}\,\mathrm{M}_\odot$. The results are displayed in Fig. 6. The top and bottom panels show the median redshift and

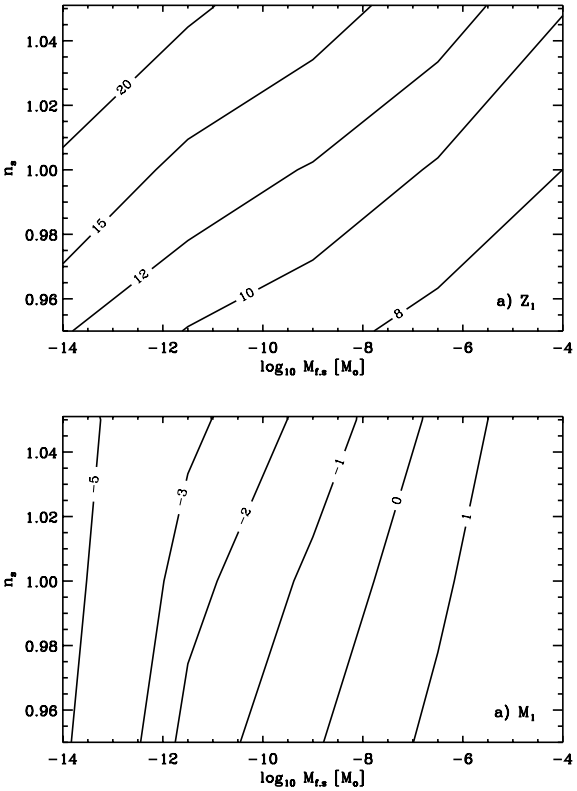

Figure 6. The median mass (M_1) and redshift (z_1) at first threshold crossing for different combinations of free-streaming mass ($M_{\rm fs}$) and primordial spectral index ($n_{\rm s}$). In the upper panel, each line indicates $z_1 = 8$, 10, 12, 15, 20 from right to left, while in the lower panel each line indicates $\log_{10} M_1 = -5, -3, -2, -1, 0, 1$ from left to right. Note that a neutralino of 100 GeV, the standard mass adopted in this paper, corresponds to a free-streaming mass of $M_{\rm fs} \sim 10^{-8}\,{\rm M}_\odot$.

the median halo mass at first barrier crossing, respectively. The impact of $n_{\rm s}$ on z_1 is interestingly strong. A 10 per cent variation has similar impact to changing $M_{\rm fs}$ by eight orders of magnitude. For example, neutralinos in a universe with $M_{\rm fs} = 10^{-14}\,{\rm M}_\odot$ and $n_{\rm s} = 0.95$ would be typically first become part of a halo at the same redshift as in a universe with $M_{\rm fs} = 10^{-5}\,{\rm M}_\odot$ but $n_{\rm s} = 1.05$. The typical mass of the first haloes is different in the two cases, however. This quantity shows a much weaker dependence on $n_{\rm s}$. The same 10 per cent variation modifies M_1 by one order of magnitude, at most. On the other hand, M_1 scales almost linearly with $M_{\rm fs}$, the two masses always differing by about seven orders of magnitude.

5 THE ASSEMBLY OF HALOES

The particle-based nature of the excursion set formalism makes it ideal to study the assembly history of dark matter haloes. As we travel along a random walk, we follow a DM particle from the very bottom of the CDM hierarchy through the successive mergers it witnesses until it ends up, e.g. in a Milky Way mass halo today. For the statistics in this section, we have modified our ensemble of trajectories so that all of them end up in a halo of similar mass to the one that hosts our own Galaxy ($M = 1.37 \times 10^{12}\,{\rm M}_\odot$).

5.1 Infall events

Fig. 7 presents the distribution of the number of infall events for all the trajectories in our ensemble of random walks. These are defined

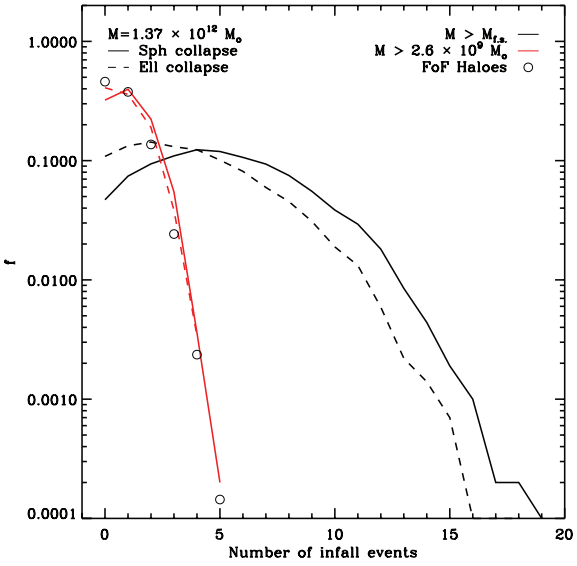

Figure 7. A histogram of the number of infall events for a random sample of all the dark matter particles that constitute a $1.37 \times 10^{12}\,{\rm M}_\odot$ halo today. Sets of curves indicate the number of infall events since the DM particles were first accreted on to any halo (black lines) or on to a $2.6 \times 10^9\,{\rm M}_\odot$ halo (red lines). Solid and dashed lines assume a constant and moving barrier, respectively. Open circles give the N-body results.

as an increase in mass by more than a factor of 2, and so are the events where the halo that hosts a given particle is accreted on to a larger system.

Black lines in Fig. 7 follow DM particles over the full hierarchy, while red lines follow them only from the moment they are hosted by a halo more massive than $2.6 \times 10^9\,{\rm M}_\odot$. The latter results can be compared directly to our N-body simulation. As in previous plots, results for both the spherical collapse barrier (solid lines) and the square root barrier (dashed lines) are shown in the figure.

If most mergers were to occur between objects of similar mass, the typical number of infall events would be very large. The difference in mass between the smallest structures and a Milky Way halo is $\simeq$20 orders of magnitude, so one might expect to see typically $20 \log_2 10 \sim 67$ infall events for each particle. Fig. 7 indicates that this is a poor representation of structure assembly in a CDM Universe. The median of the histogram is between four and five events. Thus, a typical mass element in a Milky Way halo has gone through a rather small number of events where its host halo falls into something bigger than itself. Among all these infall episodes, typically only one occurs while the particle is part of a halo larger than $2.7 \times 10^9\,{\rm M}_\odot$. This result suggests that minor mergers play an important role in the growth of dark matter haloes.

Another common misconception is that the growth of dark matter haloes is due entirely to the accretion of other haloes. From our random walks, we can assess this statement by computing the amount of mass that is formally accreted smoothly, i.e. not via mergers of any type. This quantity can be read off from Fig. 7 as the fraction of mass that has suffered zero infalls. We can see that, depending of the shape of the barrier, 5–10 per cent of the mass of a $\sim 10^{12}\,{\rm M}_\odot$ halo was accreted smoothly.

Naturally by imposing a higher mass threshold the amount of unresolved accretion increases, reaching $\sim$40 per cent when the minimum mass corresponds to the resolution limit of our N-body simulation. This matches the values we measure directly.

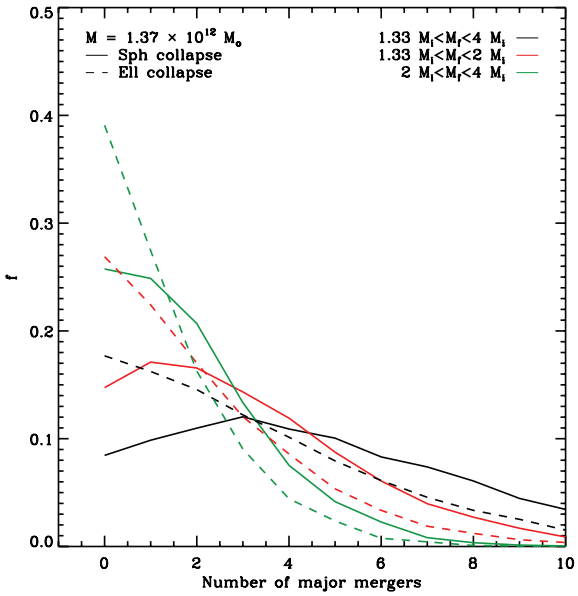

Figure 8. A histogram of the number of major mergers in which the dark matter particles of a Milky Way sized halo have been involved throughout their history. Black curves histogram the total number of major mergers experienced by the haloes containing given dark matter particles while red curves include only those major mergers where the particle is part of the larger object and green curves those where it is part of the smaller object.

The results presented in this section are weakly dependent on the mass of the final halo. Even small haloes, of about 1 $M_\odot$, have accreted 10–20 per cent of their mass smoothly and their particles have typically suffered 1–2 infall events.

5.2 The distribution of mergers

To close this section, in Fig. 8 we turn our attention to the number of major mergers that a typical DM particle that ends up in a Milky Way sized halo has experienced during its life. We define a major merger as an event in which the halo associated to a given trajectory changes its mass by a factor in the range [1.33, 4]. This represents mergers where the mass ratio of the haloes is less than a factor of 3.

The histograms displayed in Fig. 8 show that most dark matter particles have been involved in a relatively small number of major mergers. In fact, 10–20 per cent of all particles never witness a major merger. The median of the distribution is 4 for the spherical collapse model and 3 for the square root barrier.

We divide the trajectories into two categories according to the size of the halo before the merger. The first subgroup, displayed as red lines, represents the cases where the particle belongs to the larger object ($1.33M_i < M_f < 2M_i$) while green lines show the case where the particle belongs to the smaller object ($2M_i < M_f < 4M_i$). It is interesting to note that these subsets have different distributions. This implies that major mergers where the particle is part of the smaller object are more frequent than those where it is part of the larger one.

The mass cut-off induced by free streaming also produces a correlation between the redshift and the mass ratio of the progenitors. Mergers at high redshift are more likely to have low-mass ratios, while mergers between very dissimilar haloes necessarily occur only at low redshift.

6 CONCLUSIONS

We have used the excursion set formalism to examine halo formation and mass assembly in a standard ΛCDM cosmology where the DM is made of 100 GeV neutralinos. Our analytic treatment of the problem allows us to follow halo assembly histories for a large number of DM particles over more than 25 orders of magnitude in halo mass. For the first time, we are able to study halo assembly histories of DM particles from the very bottom of the CDM hierarchy up to the largest structures that exist today.

The free streaming of neutralinos induces an exponential cut-off at large wavenumbers in the primordial power spectrum. For our neutralino model, this sets 10^{-8} $M_\odot$ as the minimum mass that any dark matter halo can have. Our results suggest, however, that a very small fraction of the DM particles were ever part of a halo of mass $\sim M_{\rm fs}$. In fact, the mass of the first halo for a typical particle is comparable to the mass of the Sun. In addition, we have found that most of the matter is not part of any halo at early times; the typical redshift for first collapse is $z = 14$. Today, 5–10 per cent of the dark matter is still not part of any clump, and beyond redshift 14 most of the mass was in diffuse form. These late formation times might imply that even very low mass haloes are not expected to be strongly concentrated and thus they should be relatively easily disrupted.

The particle-based formulation of the excursion set theory allowed us to trace back to the very bottom of the CDM hierarchy the particles that today form a Milky Way sized halo. We found that there are rather few generations of accretion/merger events. Typical particles experience three or five of such episodes, only one of which occurs after the particle is part of a 10^9 $M_\odot$ halo. About 10 per cent of the mass of Milky Way sized haloes was accreted in diffuse form rather than as part of a smaller halo.

Our results depend little on the exact mass of the neutralino or on the shape of the barrier for collapse. Comparison with an *N*-body simulation suggests that the excursion set formalism gives reliable results at least over the limited mass range where a comparison can be made. Structure growth in the concordance cosmology is considerably less hierarchical than is often thought.

ACKNOWLEDGMENTS

We would like to thank Adrian Jenkins for providing us with the *N*-body simulation used in this work. We also acknowledge useful conversations with Cedric Lacey, Chung Pei Ma, Jorge Moreno, Eyal Neistein and David Weinberg.

REFERENCES

Angulo R. E., Baugh C. M., Lacey C. G., 2008a, MNRAS, 387, 921
Angulo R. E., Lacey C. G., Baugh C. M., Frenk C. S., 2008b, preprint (arXiv:0810.2177)
Bertone G., Hooper D., Silk J., 2005, Phys. Rep., 405, 279
Bertschinger E., 2006, Phys. Rev. D, 74, 063509
Bond J. R., Cole S., Efstathiou G., Kaiser N., 1991, ApJ, 379, 440
Bower R. G., 1991, MNRAS, 248, 332
Boylan-Kolchin M., Springel V., White S. D. M., Jenkins A., Lemson G., 2009, MNRAS, 398, 1150
Bringmann T., 2009, preprint (arXiv:0903.0189)
Davis M., Efstathiou G., Frenk C. S., White S. D. M., 1985, ApJ, 292, 371
Diemand J., Moore B., Stadel J., 2005, Nat, 433, 389
Gao L., White S. D. M., 2007, MNRAS, 377, L5
Gao L., Springel V., White S. D. M., 2005a, MNRAS, 363, L66
Gao L., White S. D. M., Jenkins A., Frenk C. S., Springel V., 2005b, MNRAS, 363, 379

Green A. M., Hofmann S., Schwarz D. J., 2004, MNRAS, 353, L23
Lacey C., Cole S., 1993, MNRAS, 262, 627
Lewis A., Challinor A., Lasenby A., 2000, ApJ, 538, 473
Loeb A., Zaldarriaga M., 2005, Phys. Rev. D, 71, 103520
Mahmood A., Rajesh R., 2005, preprint (astro-ph/0502513)
Moreno J., Giocoli C., Sheth R. K., 2008, MNRAS, 391, 1729
Press W. H., Schechter P., 1974, ApJ, 187, 425
Sheth R. K., Mo H. J., Tormen G., 2001, MNRAS, 323, 1
Springel V., 2005, MNRAS, 364, 1105
Springel V., White S. D. M., Tormen G., Kauffmann G., 2001, MNRAS, 328, 726
Springel V. et al., 2008, MNRAS, 391, 1685
Wechsler R. H., Zentner A. R., Bullock J. S., Kravtsov A. V., Allgood B., 2006, ApJ, 652, 71
Wetzel A. R., Cohn J. D., White M., Holz D. E., Warren M. S., 2007, ApJ, 656, 139
White S. D. M., 1996, in Schaeffer R., Silk J., Spiro M., Zinn-Justin J., eds, Cosmology and Large Scale Structure. Elsevier, Amsterdam, p. 349
Widrow L. M., Elahi P. J., Thacker R. J., Richardson M., Scannapieco E., 2009, MNRAS, 397, 1275
Zentner A. R., 2007, Int. J. Modern Phys. D, 16, 763

This paper has been typeset from a TEX/LATEX file prepared by the author.